AIAA JOURNAL
Vol. 47, No. 9, September 2009

Localization of a Breathing Crack Using Super-Harmonic Signals due to System Nonlinearity

F. Semperlotti*
Pennsylvania State University, University Park, Pennsylvania 16802
K. W. Wang†
University of Michigan, Ann Arbor, Michigan 48109
and
E. C. Smith‡
Pennsylvania State University, University Park, Pennsylvania 16802

DOI: 10.2514/1.38947

In this paper, a new damage detection technique able to identify the location of a breathing crack in an isotropic rod, relying only on real-time measurements, is proposed. The detection algorithm exploits the phase information associated with the superharmonic components produced, in the Fourier spectrum, by the nonlinear dynamic response of this kind of defect under the influence of an external dynamic excitation. The validity of the proposed algorithm for a weakly nonlinear system is supported by an analytical solution for a cracked beam obtained through the harmonic balance approach. A numerical investigation is conducted by means of a finite element model of an isotropic beam integrating nonlinear contact elements in the damaged area and solved for the steady-state response. Three different postprocessing approaches, incorporating the proposed damage detection algorithm, are formulated and compared to assess the capability of the current methodology. Results from the cracked beam model clearly show the generation of the superharmonics as a result of the nonlinear dynamic behavior of the breathing crack. The phase associated with the superharmonic components is then processed through the detection algorithm and the predicted location is compared with the actual position of the defect to assess the performances of the methodology.

Nomenclature

A	=	beam cross-sectional area
B, C	=	constant of integration
C	=	damping matrix
D_n, D_{0n}	=	spectral coefficients
$\mathbf{d}_c$	=	vector identifying the crack location
E	=	Young's modulus
F_n	=	force amplitude at the nth frequency component
$F(t)$	=	time varying forcing function
$f_c(t)$	=	restoring force of the nonlinear spring
$G_k(ik\omega)$	=	transfer function at the kth harmonic
$H[u_C(t)]$	=	Heaviside unit function
i	=	complex unit
K	=	stiffness matrix
K_C	=	stiffness of the nonlinear spring
K_{op}	=	local stiffness for crack in open configuration
k	=	index of the harmonic component
k_n	=	wave number correspondent to the frequency ω_n
L	=	distance between sensors 1 and 2
L_r	=	total length of the rod
L_w	=	length of the boxcar window
M	=	mass matrix
u_C	=	relative displacement of the two endpoints of the axial spring
u_m, u_n	=	endpoint displacements of the nonlinear spring
$u(x, t)$	=	axial displacement field
x_1, x_2	=	crack distance from sensors 1 and 2
Γ_k	=	phase due to the traveling wave
ΔT	=	integration time step
$\Delta\varphi_n$	=	relative phase difference for the nth superharmonic
δ_k	=	initial phase of the spring restoring force
φ_{0n}	=	initial phase
φ_{1n}, φ_{2n}	=	measured phase at sensors 1 and 2
Ψ_k	=	measured phase
ω	=	frequency
ω_n	=	nth frequency component

Received 5 June 2008; revision received 6 April 2009; accepted for publication 10 April 2009. Copyright © 2009 by the American Institute of Aeronautics and Astronautics, Inc. All rights reserved. Copies of this paper may be made for personal or internal use, on condition that the copier pay the $10.00 per-copy fee to the Copyright Clearance Center, Inc., 222 Rosewood Drive, Danvers, MA 01923; include the code 0001-1452/09 and $10.00 in correspondence with the CCC.

*Ph.D. Student in Aerospace Engineering. Student Member AIAA.
†Department Chair and Stephen P. Timoshenko Professor of Mechanical Engineering. Member AIAA.
‡Professor of Aerospace Engineering. Member AIAA.

I. Introduction

THE interest in detecting structural damages at the earliest possible stage has always been a major issue in the structural health monitoring community. The introduction of a sensitive and efficient damage detection system to monitor the health of an in-service structure would result in a considerable improvement in the performance and safety of the mechanical system and/or in a drastic decrease of its maintenance cost.

Many different damage detection approaches, relying on the analysis of different physical phenomena and experimental data, have been investigated in the past to get information able to identify the level of integrity of a mechanical system. Extensive reviews of the damage detection methodologies proposed in the past can be found in [1–4]. Many of the successful global damage detection methodologies normally rely on the use of a baseline signal of the healthy structure and/or require an accurate structural model (e.g., finite element model) with a model updating approach. The application of these techniques to perform a continuous monitoring of an in-service structure, however, undergoes some important limitations.

The use of a baseline signal, in fact, can be particularly cumbersome, especially if we want to achieve a high level of accuracy. Moreover, if the damage detection effort has to be performed while the mechanical system is in operating conditions, this would require developing multiple databases corresponding to the different regimes [5]. In a similar fashion, the model updating approach could be difficult to implement. This class of methods

requires the development of an accurate finite element model of the healthy structure, which is normally a very challenging task to achieve for complex mechanical systems. This aspect becomes even more challenging if we are interested in the structural response in high-frequency ranges. Moreover, the model updating methods are generally very time consuming and require considerable computational resources.

II. Problem Statement and Research Objectives

For the preceding reasons, the present paper aims to investigate a new approach in which the location of a breathing-crack-type defect can be detected through real-time measurements, without relying on a baseline signal or on a finite element model of the structure.

In the past few years, researchers [6,7] have already pointed out the peculiar behavior of a structure with a breathing crack excited by an external dynamic load. The frequency spectrum of its nonlinear structural response, in fact, shows the appearance of higher order harmonics that are integer multiple or fractional multiple of the driving frequency. These harmonics are commonly denominated superharmonics and subharmonics, respectively. A more specific denomination of these harmonic components (ultrasubharmonics, combinational tones, etc.) can be used to characterize their origin and relation with both the driving frequency and the structural modes [8].

These higher order harmonics are generated at the crack location due to the crack's opening and closing mechanism triggered by the external dynamic excitation. These waves, identified by very specific frequencies, travel through the structure carrying with them the information about the spatial origin of the wave source. Once the wave is generated, in fact, the phase associated with the signal varies, in a linear structure, linearly with the distance traveled by the wave. By properly processing the time signal and the associated phase information at two different locations in the structure, we can identify the spatial origin of the wave source, that is, the location of the crack. This approach is, in principle, suitable to detect cracks at their earliest stage where they already exhibit the aforementioned nonlinear behavior, but are still too small to be detected with global vibration-based damage detection techniques. Also, although the proposed method uses an excitation load in the low ultrasonic frequency range, it does not require solving, as frequently happens with the ultrasonic-based approaches, for the entire wave field, which usually requires the knowledge of the reflection and transmission coefficients.

Based on this specific nonlinear behavior of a breathing crack, this paper will present a methodology to determine the location of the defect by exploiting the information associated with the superharmonics components present in the spectrum of the nonlinear structural dynamic response.

III. Approach

To illustrate the proposed approach without losing generality, a rectangular isotropic beam with free–free boundary conditions is used as a test bed structure in this study. A single fatigue-crack-type defect is assumed to be developed by the structure as a consequence of a high cycle fatigue environment. Under this assumption, the structure can be considered linear in terms of mechanical properties, except for a very small area close to crack tips where the material undergoes plastic deformations. At its earliest stage, the crack can reasonably be considered in a closed configuration, that is, the two sides of the crack stay in contact at the initial instant. We believe that, although the results shown in this paper deal with the specific crack's configuration described earlier, the proposed damaged detection algorithm will still be valid either for low cycle fatigue cracks (unless there are extended plastically deformed areas in the structures producing considerable fluctuations in the wave velocity) or for crack exhibiting an initial opening as far as the external dynamic excitation is able to induce the "breathing" of the crack.

As already demonstrated by other researchers, a fatigue crack exhibits a peculiar behavior when excited by a dynamic load. The excitation, in fact, forces the crack to open and close (commonly referred as to breathing) and the resulting clapping of the crack's edges produces harmonics that are integer multiple or fractional multiple of the forcing frequency. These harmonics are commonly referred as to superharmonics and subharmonics, respectively.

The damage detection technique proposed in this paper exploits the specific information carried by the superharmonic components produced by the crack's nonlinear response to a prescribed external dynamic excitation. The steady-state part of the time response is processed through three different data postprocessing approaches, all integrating the same localization algorithm, but relying on different analytical principles to extract the parameters relevant to the crack location. A finite element model is developed to simulate the beam's structural response and to create a database of results, which will be successively used to test the proposed damage detection algorithm. It is important to note that this model is not a part of the identification procedure but is just a means to generate the input data necessary to test and illustrate the detection algorithm.

In summary, this paper is organized as follows:

1) A damage detection technique able to identify the location of a breathing crack is proposed along with its analytical formulation.

2) Three different data postprocessing procedures are developed and compared. These procedures integrate the same damage detection algorithm but rely on different approaches to extract, from the steady-state structural response of the damaged structure, the input needed to implement the localization algorithm formulated.

3) The nonlinear behavior of an isotropic structure including a breathing-crack-type defect is simulated through a finite element (FE) model integrating nonlinear contact elements. The damage detection algorithm along with the three data postprocessing approaches is numerically tested through the data produced by the nonlinear FE model for five different crack locations.

A. Localization of an Unknown Wave Source

The damage localization technique presented in this paper is synthesized based on the algorithm proposed by Doyle [9,10] to determine the location of an unknown dispersive pulse in an isotropic beam. The algorithm was originally formulated to determine the spatial location of an external impact using strain measurements.

For the purpose of damage localization, we first derive an algorithm to determine the spatial location of an unknown wave source generating a continuous nondispersive longitudinal wave in an isotropic rod.

Given the rod in Fig. 1, subjected to an external longitudinal dynamic load and assuming the origin of the longitudinal axis coincident with the point of excitation, the equation of motion can be written as

$$EA\frac{\mathrm{d}^2u}{\mathrm{d}x^2} + \omega^2\rho A u = 0 \tag{1}$$

Whereas, the boundary condition is

$$EA\frac{\partial u(x,t)}{\partial x} = F(t) \quad \text{at } x = 0 \tag{2}$$

Considering the well-established general solution of the homogenous wave equation in spectral form,

$$u(x,t) = \sum Be^{-i(kx-\omega t)} + \sum Ce^{i(kx+\omega t)} \tag{3}$$

Using Eqs. (2) and (3), the solution for the outward moving wave can be written as

$$u(x,t) = -\frac{1}{2EA}\Sigma_n\frac{\hat{F}_n}{ik_n}e^{-i(k_nx-\omega_n t)} \tag{4}$$

where $u(x,t)$ is the displacement in each of the two sides of the rod at time t and location x, E is Young's modulus, A is the cross-sectional area of the rod, k_n is the wave number corresponding to the frequency ω_n, F_n is the spectral amplitude of the external force, and i is the imaginary unit.

To emphasize the relation between the phase terms, Eq. (4) can be written as

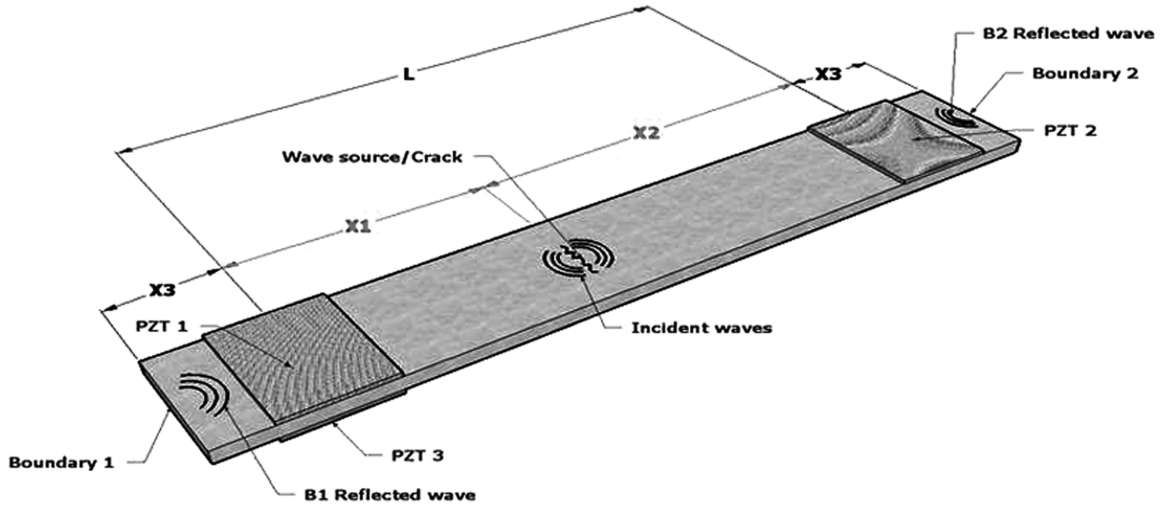

Fig. 1 Schematic of a rod with a wave source in an unknown location.

$$D_n e^{i\varphi_n} = D_{0n} e^{i\varphi_{0n}} e^{-ik_n x} \tag{5}$$

Where D_n and D_{0n} are constant coefficients describing the amplitude, and φ_n, φ_0, and $k_n x$ represent the measured phase at location x, the initial unknown phase of the excitation, and the change in phase due to the propagating wave, respectively.

We can extract, from Eq. (5), the relation between the measured phase and the location x of the applied force as follows:

$$\varphi_n = \varphi_{0n} - k_n x \tag{6}$$

Inverting Eq. (6) with respect to x gives the basic relation to find the location of the wave source:

$$x = \frac{1}{k_n}(\varphi_{0n} - \varphi_n) \tag{7}$$

Equation (7) provides the distance x between the origin of the reference system (previously assumed coincident with the source location) and the point where the phase φ_n is measured. This equation has two unknowns, x and φ_{0n}, and therefore cannot be directly solved for the location of the source. To overcome this problem, we can use two measurement points, one on each side of the source. Writing Eq. (7) for the two different points and knowing the absolute distance between the sensors, we get the following set of equations:

$$x_1 = \frac{1}{k_n}(\varphi_{0n} - \varphi_{1n}) \quad x_2 = \frac{1}{k_n}(\varphi_{0n} - \varphi_{2n}) \quad x_1 + x_2 = L \tag{8}$$

Finally, eliminating the initial phase φ_{0n}, we get

$$\begin{aligned} x_1 &= \frac{1}{2}L - \frac{1}{2k_n}(\varphi_{1n} - \varphi_{2n}) = \frac{1}{2}L - \frac{\Delta\varphi_n}{2k_n} \\ x_2 &= \frac{1}{2}L + \frac{1}{2k_n}(\varphi_{1n} - \varphi_{2n}) = \frac{1}{2}L + \frac{\Delta\varphi_n}{2k_n} \end{aligned} \tag{9}$$

It has to be noted that, before solving Eq. (9), the measured phases φ_{1n} and φ_{2n} have to be unwrapped. In this way, the ambiguity at $\pm\pi$, produced by the arctangent function when calculating the phase, can be easily overcome.

It clearly appears, from Eq. (9), that the source location is calculated estimating the difference in the path length traveled by the outward moving waves to the sensors. This means that, for an accurate localization of the source, both magnitude and sign of the $\Delta\varphi_n$ are equally important. This observation will be important when comparing the performances of the different postprocessing approaches.

We must note, also, that Eq. (9) is derived considering only the outward moving wave from the source. Therefore, this set of equations would give, theoretically, the exact estimate of the source location if we considered an unbounded structure where the propagating signal hits the sensors only once. In a finite structure, however, boundaries produce reflected waves that propagate back toward the sensors, giving additional phase contributions. In a linear behaving structure, this problem has been overcome acquiring only the first passage of the initial signal [9,10] and appending the long-term theoretical solution for the beam dynamic response. This procedure allows one to get a good estimate of the spectral content while removing the effects of the reflected waves.

In this paper, however, we investigate a different approach where the following applies:

1) The spectral content is estimated from the acquired steady-state response including, therefore, boundary and crack reflections. The reason for considering the steady state is due to the fact that the initial transient response does not necessarily include the superharmonic components.

2) The host structure is weakly nonlinear; therefore, there is not a close-form solution which could be used to append the long-term response to the measured data.

B. Breathing Crack as a Source of Excitation

As already stated in Sec. III, a structure including a breathing-crack-type defect exhibits a characteristic behavior when subjected to an external dynamic excitation. In particular, the external load produces tensile and compressive stresses on the two edges of the crack, leading to a continuous (eventually periodic) opening and closing of the crack, usually referred as breathing. The impact produced by the clapping of the two edges, when subjected to compressive stresses, creates new wave fronts for which the frequencies are integer multiples or fractional multiples of the driving frequency associated with the external dynamic load. This behavior suggests that the breathing crack can be considered as a source of excitation whose spectrum contains the driving frequency plus its superharmonic and/or subharmonic components. Under this assumption, the crack behaves as a wave source similar to what was shown in Sec. III.A. It follows that processing the phase information associated with the higher order harmonic components, in a similar fashion as illustrated by Eq. (9), will result in locating the position of the superharmonics source that, ultimately, is the spatial location of the crack.

It has to be noted, however, that, in this case, the dynamic response of the structure is nonlinear due to the presence of the breathing crack. The crack is, in fact, associated with a localized change in the stiffness value. When the crack is open, due to a tensile stress state, the local stiffness drops at a value K_{op}, whereas, when the crack is closed due to a compressive stress state, the local stiffness is restored

to the value $K > K_{op}$ associated with the healthy structure. When the system is excited by an external dynamic excitation, which alternates compressive and tensile stress states on the crack, the continuous opening/closing behavior of the crack induces a periodic change in the local stiffness (between the limit value K and K_{op}) which determines the nonlinear character of the overall dynamic response. Nevertheless, a small breathing crack produces small changes in the stiffness matrix, making the system weakly nonlinear [11,12] and usually assuring the existence of a steady-state periodic solution. Therefore, to extend the algorithm described in Sec. III.A to the present structure, we need to derive the phase-based relation, equivalent to Eq. (9), valid for the steady-state response of a weakly nonlinear system.

In this study, the external dynamic load is assumed to be a single frequency periodic excitation applied in the longitudinal direction, so that the dynamic response of the structure can be described according to the wave propagation in rods. The other assumptions are as follows:

1) The clapping of the crack, produced by the external dynamic excitation, takes the place of the wave source (i.e., external impact) considered in Sec. III.A.

2) The crack can be considered as a weak nonlinearity and the steady-state solution is almost periodic.

3) The dynamic response of the structure under the external axial load can be described according to the wave propagation theory in rods.

C. Harmonic Balance Solution of a Weakly Nonlinear Rod

The first step involved in the extension of Eq. (9) to determine the crack location in a weakly nonlinear system consists of evaluating the phase relation, under steady state, between the wave source/crack location and another point in the structure.

According to Musil [13], the dynamic response of a structure including a breathing crack can be calculated using a finite element model where the breathing crack is modeled through a piecewise linear spring. The system can be described by the following dynamic equation:

$$M\ddot{u}(t) + C\dot{u}(t) + Ku(t) + f_C(t) = F(t) \tag{10}$$

where M, C, and K represent the mass, damping, and stiffness matrices, $f_C(t)$ is the restoring force produced by the spring with piecewise linear stiffness, and $F(t)$ is the external applied dynamic load. The piecewise linear spring allows taking into account the opening/closing behavior of the crack which, as explained before, is associated with a change into the local stiffness, which switches periodically between the open crack K_{op} and the closed crack K values. In this study, we consider an axial spring because we are only interested in the longitudinal response of the structure.

The effect of the spring can be expressed in the following way:

$$f_C(t) = K_C[u_n(t) - u_m(t)]\mathbf{d}_c = K_C u_C(t)\mathbf{d}_c = K_C u_C(t)H[u_C(t)]\mathbf{d}_c \tag{11}$$

where $u_C(t) = [u_n(t) - u_m(t)]$ represents the relative axial displacements of the two endpoints of the nonlinear spring (i.e., the two edges of the crack) having a stiffness K_C. $H[u_C(t)]$ is the Heaviside unit function used to localize the stiffness change, whereas $f_C = 0$ represents the unchanged stiffness condition (crack closed) and $F_C = K_C u_C(t)$ represents the stiffness decrease due to the crack opening. The vector $\mathbf{d}_c = [0, \ldots, 1, \ldots, 1, \ldots, 0]^T$ characterizes the location of the crack.

To calculate the steady-state response of this nonlinear system, the harmonic balance approach can be applied to the system of Eqs. (10) and (11). The dynamic excitation can be expressed in Fourier series as follows:

$$F(t) = \sum_k F_k e^{i(k\omega t + \varphi_k)} \quad \text{for } k = 0, 1, 2, 3, \ldots \tag{12}$$

where F_k, $k\omega$, and φ_k represent the amplitude, frequency, and phase of the kth harmonic of the excitation load, respectively.

Following the same approach, we can expand the displacement field in Fourier series:

$$u(t) = \sum_k u_k e^{i(k\omega t + \psi_k)} \quad \text{for } k = 0, 1, 2, 3 \ldots \tag{13}$$

The restoring force f_c can be approximated through the Fourier series [11] as

$$f_c(t) = \sum_{k=0}^{\infty} f_{ck}[\cos(k\omega t) + \delta_k] \quad \text{for } k = 0, 1, 2, 3 \ldots \tag{14}$$

Substituting the Eqs. (12–14) in Eq. (10), we obtain an expression valid for the kth harmonic:

$$e^{i\Psi_k} u_k - G_k(ik\omega)e^{i\varphi_k} F_k = -f_{ck} e^{i\delta_k} e^{i\Gamma_k} g_{ck}(k\omega) \tag{15}$$

where $G_k(ik\omega)$ represents the transfer function of the mechanical system for the kth harmonic and can be expressed as

$$G_k(ik\omega) = (K + ik\omega C - k^2\omega^2 M)^{-1} \tag{16}$$

The term $f_{ck}e^{i\delta k}$ represents the kth harmonic of the restoring force produced by the axial spring, whereas $e^{i\Gamma k} g_{ck}(k\omega)$ is a term related to the location of the spring. The term $e^{i\Gamma k} g_{ck}(k\omega)$ is obtained from

$$e^{i\Gamma k} g_{ck}(k\omega) = g_{ck}(ik\omega) = G_k(ik\omega)d_c$$

Equation (15) represents the equilibrium equation for each harmonic at the steady state for a weakly nonlinear system. From Eq. (15), we can extract the relation that holds at the steady state, and for each harmonic between the phase of the displacement, the applied external force and the crack's restoring force. Noting that the applied external force is chosen to be a periodic function at a specific frequency ω, F_k in Eq. (12) is different from zero only for $k = 1$ which corresponds to a periodic signal of frequency ω. Therefore, the phase relation at the superharmonic frequencies (i.e., for $k = 2, 3, 4, \ldots$) is given by

$$\Psi_k = \delta_k + \Gamma_k \tag{17}$$

where Ψ_k is the phase associated with the measured displacement, δ_k is the initial unknown phase of the spring restoring force, and Γ_k is a phase associated with the spatial location of the crack and therefore is a function of the longitudinal coordinate x. Observing that the considered structure has a linear behavior, except for the area located around the crack, we can assume that the phase Γ_k will vary as $\Gamma_k(x) = -k_n x$ according to the longitudinal wave propagation theory in linear structure. With these assumptions, it can be noted that Eq. (17) is equivalent to Eq. (6) extending, therefore, its range of applicability to the steady-state solution of a weakly nonlinear rod.

It should be noted that all the phases are calculated with respect to the external excitation.

D. Optimal Sensor Placement

Although Eq. (17) states that the phase measurement can be performed at any point on the structure, it can be shown that the location of the sensors plays a major role in the performance of the proposed localization algorithm. Table 1 shows the phase change, at the sensor locations, occurring to the traveling wave after each reflection when the sensors are located symmetrically with respect to the boundaries, as in Fig. 1. We can observe how the absolute value of the phase difference is always constant while, at the even-order reflections, the $\Delta\varphi$ changes sign. Note that, for simplicity, the initial phase φ_{0n} is omitted because this constant term cancels out when calculating the phase difference $\Delta\varphi$.

We must observe that, even if the phase difference occurring at the even-order reflections changes sign, the corresponding amplitude is

Table 1 Change in phase following the reflections; $m = 2, 4, 6, \ldots$ indicates the order of the even-order reflections

	Sensor 1	Sensor 2	Phase difference $\Delta\varphi = \varphi_2 - \varphi_1$
Incident wave	$k_n x_1$	$k_n x_2$	$k_n(x_2 - x_1)$
First reflected wave	$k_n x_1 + 2k_n x_3$	$k_n x_2 + 2k_n x_3$	$k_n(x_2 - x_1)$
Second reflected wave	$2k_n x_2 + 4k_n x_3 + k_n x_1$	$2k_n x_1 + 4k_n x_3 + k_n x_2$	$-k_n(x_2 - x_1)$
$(m-1)$th reflections	$(m-1)k_n x_1 + 2(m-1)k_n x_3 + (m-2)k_n x_2$	$(m-1)k_n x_2 + 2(m-1)k_n x_3 + (m-2)k_n x_1$	$k_n(x_2 - x_1)$
mth reflections	$mk_n x_2 + 2mk_n x_3 + (m-1)k_n x_1$	$mk_n x_1 + 2mk_n x_3 + (m-1)k_n x_2$	$-k_n(x_2 - x_1)$

always lower than the $(m-1)$ odd-order reflections (because they traveled a larger distance), where m represents the even-order reflections. Consequently, even if the overall amplitude will be affected, the resulting phase difference $\Delta\varphi$ will keep the same sign determined by the incident waves. On the contrary, if the sensors are not symmetrically located with respect to the boundaries, the phase difference associated with the odd-order harmonics changes also in absolute value. Even if the wave resulting from the superposition of the odd-order reflected waves will have small amplitude (when considering a sufficient number of reflections), the associated phase difference can still produce a shift on the measured $\Delta\varphi$ that can considerably affect the performance of the detection algorithm.

These simple considerations show that, to minimize the effect of the reflected waves, the sensors must be placed in a symmetric configuration with respect to the boundaries, as shown in Fig. 1. Similar considerations apply also to the phase balancing of the waves reflected from the crack interface and from the far ends of the sensors, respectively.

For the crack interface, it is assumed that their contributions to the overall phase is negligible because the crack area A_c is small compared to the cross-sectional area A of the rod ($A_c/A < 10\%$). Also, the reflections taking place at the far ends of the sensors can be neglected. Reflected waves from the sensors are symmetric with respect to the boundaries (therefore, rules at Table 1 apply similarly as shown for the case of boundary reflections) and their amplitude is negligible due to the small interface area between sensor and structure.

E. Structural Finite Element Model

To test the algorithm described by Eq. (17), a finite element model of a beam including one breathing crack has been developed. The test structure is a rectangular shaped beam in aluminum 6061 T6511. The geometrical and mechanical properties are as follows: the length, width, and thickness are 0.2, 0.008, and 0.0026 m, respectively; Young's modulus is 68.94 GPa, density ρ is 2700 Kg/m^3, and Poisson's ratio v is 0.33.

The finite element model, shown in Fig. 2a, has been built through the commercial FE software Patran using 3D hexahedral 8 nodes linear solid elements.

To reproduce as close as possible the behavior of a breathing crack, nonlinear gap elements have been added between the two edges of the crack. The gap element acts essentially as a bilinear spring with zero stiffness when the end nodes have a positive relative displacement (i.e., when the crack is subjected to a tensile load) or with a theoretical infinite stiffness when undergoing a negative relative displacement (i.e., when the crack is subjected to a compressive load). This gap element allows the two sides of the crack 1) to close, remaining in touch with each other and avoiding any material overlapping, when they are subjected to a compressive load (Fig. 2b), and 2) to freely open when they are subjected to a tensile load (Fig. 2c).

The external dynamic excitation needed to interrogate the system is assumed to be produced by piezoelectric patches bonded onto the host structure. These transducers, however, are not physically modeled (this is a reasonable assumption considering that their mass is negligible with respect to the mass of the host structure), although the excitation produced by these actuators is taken into account through a frequency-dependent dynamic load acting along the boundary of the patch itself. This load is intended to simulate the high frequency dynamic excitation produced by the piezoelectric actuator when driven with a sinusoidal voltage at a prescribed frequency.

Three piezoceramic transducers (PZTs) are used to interrogate and to sense the dynamic response of the structure. In particular, the actuators labeled as PZT 1 and 3, depicted in Fig. 2a, are used to excite the structure simulating an axial dynamic load. PZT 1 and 2, instead, are used to collect the dynamic response of the rod. Based on this modeling approach, different crack configurations will be analyzed.

F. Nonlinear Time Response Analysis

The previously described FE model is used to simulate the time response of the damaged structure excited by a continuous sinusoidal load. Further information about the selection of the driving frequency will be provided later on in this paper.

The FE model has been solved for the nonlinear time response through the commercial finite element solver Nastran, using a step-by-step integration algorithm. A 0.5 μs time step, corresponding to a Nyquist frequency of 500 kHz, has been used and the integration has been carried on up to 80 ms. Also, a structural damping of 2% has been applied. At each time step, the structural response is collected in terms of velocity at the edge of PZT 1 and 2, depicted in Fig. 2a as output 1 and 2.

To obtain the spectral content of the structural response, the steady-state part of the solution is processed through the discrete Fourier transform. An example of the time response, collected from the PZT1, along with its spectral content, is shown in Fig. 3, both for the healthy and the damaged configuration. A direct comparison of Figs. 3b and 3d reveals that the presence of the crack is associated with the appearance of superharmonic components at frequencies that are even-integer multiple of the forcing frequency. This is a

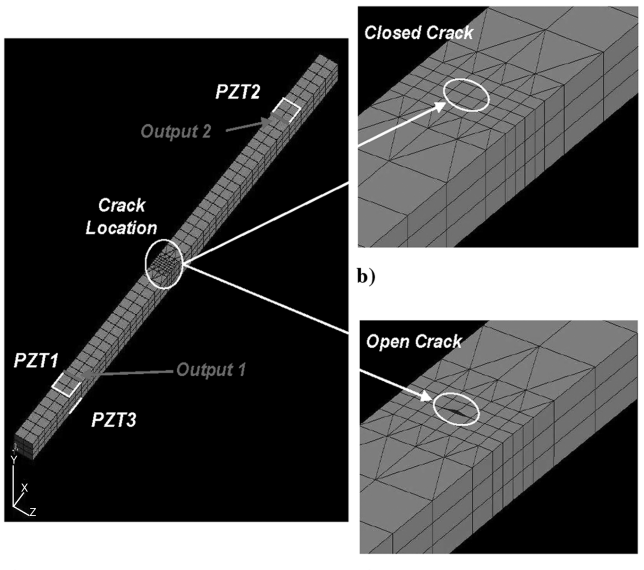

Fig. 2 Finite element model of the isotropic beam, including a) a breathing crack, which assumes b) closed or c) opened configurations depending on the local stress distribution.

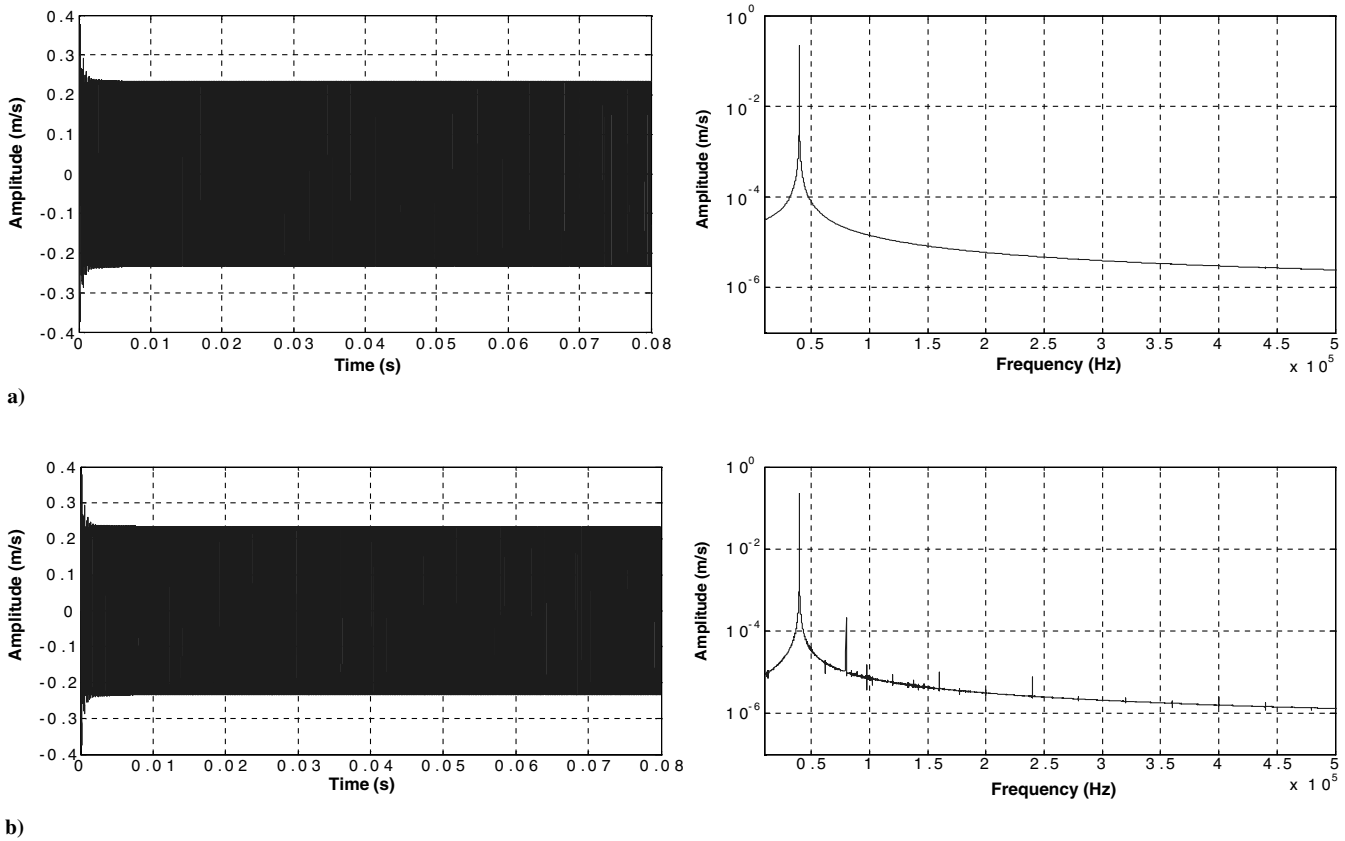

Fig. 3 Time response and spectral content at sensor 1: a) healthy structure, b) damaged structure.

phenomenon typical of a breathing crack as also reported by other authors [14–16].

G. Selection of the Driving and Superharmonic Frequencies

The selection of the driving frequency of the external load, used to interrogate the structure, is a key parameter in determining the performance of the detection algorithm. Although a detailed analysis of the optimal driving frequency is not in the scope of this paper, some considerations have to be drawn to obtain a good estimate of the crack location.

According to the general theory of nonlinear dynamic systems [8,17], to maximize the amplitude of the response of the superharmonic components, the driving frequency Ω should be close to $\Omega = \omega_n/m$, where m is an integer number and ω_n is the nth structural modes. This simple rule would suggest selecting a driving frequency for which the correspondent superharmonic is as close as possible to a structural mode. However, the proposed damage detection algorithm implies some limitations on the selected frequencies, preventing us from simply choosing the driving frequency according to the previous consideration.

In the original version of this algorithm [10], each frequency guarantees, ideally, the identification of the location of the impact point. At the natural frequencies, however, the discontinuity in the phase produces considerable oscillation in the estimated phase and, consequently, in the estimated location. Therefore, frequencies corresponding to natural modes should be kept, as much as possible, out of the set of data used to estimate the location. Because this observation still holds for the proposed damage detection algorithm, it becomes evident that the choice of the driving frequency derives from a tradeoff between getting a high-amplitude superharmonic response and a superharmonic frequency that does not overlap with a structural mode.

Another key observation concerns the frequency components that have to be retained in the database used as input for Eq. (17). In the present approach, the information about the location of the crack is carried only by the superharmonic components, those being the only harmonics generated at the crack interface. For this reason, the location of the crack will be correctly estimated only at those frequencies corresponding to a superharmonic. Moreover, the driving frequency has to be discarded because it is mainly generated at the transducer's location. This is also demonstrated by the analytical simulations where, using the phase associated with the driving frequency, Eq. (17) estimates the location of the wave source very close to actuators 1 and 2.

It can be noted how the set of exploitable data for the damage identification is now extremely reduced, especially if compared with the one available in the original version of this algorithm where each frequency could be effectively processed. This problem will be addressed in the next paragraph where three possible data postprocessing techniques are developed and compared.

IV. Data Postprocessing Procedures

Data postprocessing has already been proven to be a major issue in structural health monitoring. Because we are generally interested in detecting the damage at its earliest possible stage, the changes in the parameters are typically very small. These changes can often be masked either by the experimental noise or simply by the overall structural response of the system in the case where it is slightly affected by the structural damage. This can lead to an inaccurate characterization or to a completely erroneous estimation of the flaw, even if the damage detection algorithm itself is effectively sensitive to the defect. For these reasons, a proper data postprocessing procedure able to extract features directly related to the presence of the damage becomes of crucial importance to guarantee the performances of the damage detection algorithm.

To the sources of error, previously cited, we must add a third cause that is directly related to the nature of the proposed algorithm. As discussed in Sec. III.D, the wave fronts reflected from the boundaries travel back toward the sensors giving an additional phase contribution that, if not taken into account, can considerably corrupt

the accuracy of the estimated location. A possible way to contain the effects of the reflected waves has already been discussed in Sec. III.D and is based on a proper placement of the sensors. However, it has to be noted that, because the detection algorithm relies on the phase difference at two different locations, it is intrinsically robust against additional constant phase terms that cancel out once evaluating Eq. (9). Nevertheless, errors in the evaluation of the relative phase difference $\Delta\varphi$ can significantly affect the estimated damage location, so that a specific data postprocessing procedure is still needed to extract the phase information with sufficient accuracy.

For these reasons, three different data postprocessing techniques have been developed and compared to evaluate their performances on the phase-difference estimation and on their robustness against undesired reflections. In particular, the proposed postprocessing techniques, described hereafter, are based on 1) discrete Fourier transform (DFT), 2) cross transfer function (CTF), and 3) Hilbert transform (HT).

The first two approaches (DFT and CTF) have been historically used to evaluate the spectral content and the cross correlation between two time signals. However, it will be demonstrated in the following paragraphs how these techniques do not provide enough accuracy and data points to be effectively used in conjunction with the proposed damage detection algorithm. The Hilbert transform, instead, provides an extended data set for each frequency, thanks to its capability to retain the time information. Moreover, it will prove to be much more robust to the effects of wave reflections and windowing parameters.

This concept will be further clarified in the following paragraphs.

A. Discrete-Fourier-Transform-Based Approach

The first data postprocessing approach, discussed in this paper, relies on the use of the discrete Fourier transform to evaluate the phase content associated with the signal collected at each sensor. A block diagram illustrating the sequence of operations needed to estimate the crack location is showed in Fig. 4.

The output collected at the two sensors, labeled as output 1 and 2, are first processed through a moving window, then fed into the DFT block to estimate the phase associated with each frequency component. Successively, the phase associated with the super-harmonics is extracted from the spectrum and the $\Delta\varphi$ is estimated. The relative phase difference $\Delta\varphi$ is used as input for the damage detection algorithm to estimate the crack location $x_{c,n}$ associated with the nth windowed signal. Finally, the result is stored into an array and the procedure is iterated over n windowed signals. Once the nth iteration is completed and the array of the estimated locations is completely filled in, the $x_{c,n}$ are linearly averaged to provide the final estimate of the crack location x_c.

The mechanism of the moving window (conceptually similar to a moving average) is illustrated in Fig. 5. The overall time response is windowed with a boxcar window of length L_w and the first iteration is carried on. Then, the window is moved $(n-1)/2$ times forward and backward, respectively, by a quantity equal to Δt (assumed equal to ΔT in these calculations) while the crack estimate is performed at each step. Because one of the main goals of the moving window is to minimize the effect of the reflections, L_w is chosen to be an even-integer multiple of the time of flight (ToF) of the wave. The ToF is defined as the time needed for the wave to travel a distance equal to the length L of the rod. In this way, taking $L_w = 2 \cdot n \cdot \text{ToF}$ each reflected wave strikes n times both the sensors and comes back to the starting position. This procedure allows containing the impact of the reflected wave over the estimated phase because, when performing the $\Delta\varphi$ calculation, these contributions cancel out almost completely.

Also, at each iteration, the window is moved (forward or backward) a step equal to the integration time step used for the nonlinear time response ($\Delta T = 5.\text{E}-7$ s), whereas the total number of windows is chosen to be equal to an even-integer multiple of the ToF. This procedure is intended to limit the effects of the waves close to the edges of the window that most likely are not balanced in a single iteration. Once the entire set of estimated locations is generated through this moving window approach, the set of values is linearly averaged to produce the final estimate of the crack location.

B. Cross-Transfer-Function-Based Approach

The second data postprocessing approach investigated in this paper is based on the cross transfer function (CTF) concept to

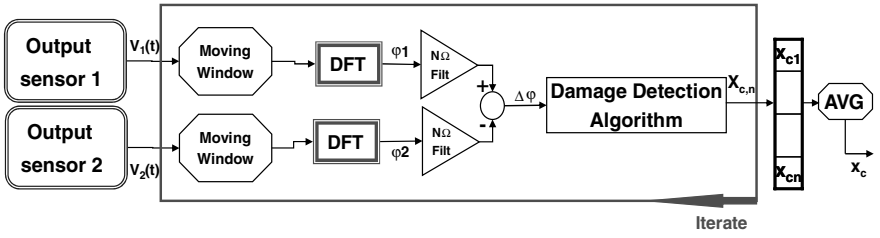

Fig. 4 Block diagram of the discrete-Fourier-transform-based approach.

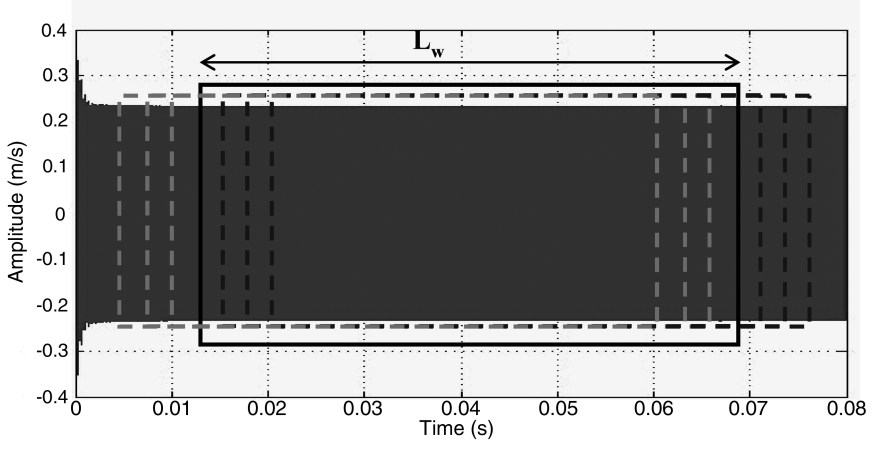

Fig. 5 Schematic of the moving window procedure.

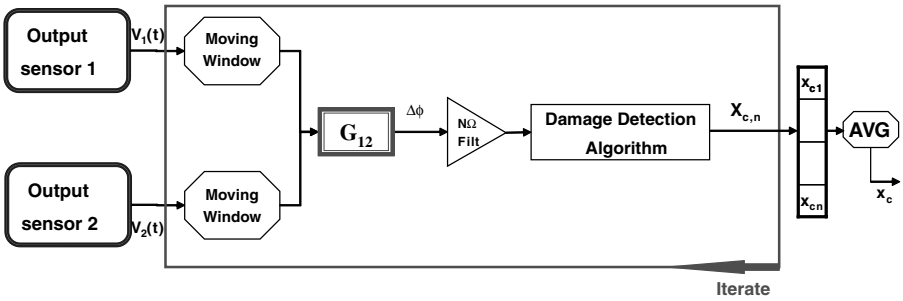

Fig. 6 Block diagram of the cross-transfer-function-based approach.

estimate the relative phase $\Delta\varphi$ between the two signals. The block diagram illustrating the data flow is showed in Fig. 6.

This approach is similar to the DFT-based approach except that the relative phase difference $\Delta\varphi$ is now estimated calculating the cross transfer function between the signals, collected at the two sensors and extracting the phase associated with the CTF, which results to be the phase difference between the two signals.

The block labeled G_{12} in Fig. 6 calculates the cross transfer function according to the following relation:

$$G_{12} = \frac{P_{12}(f)}{P_{11}(f)}$$

where $P_{12}(f)$ is the cross power spectral density between the two measured signals, and $P_{11}(f)$ is the autospectral density of the signal collected at sensor 1.

The same considerations discussed in Sec. IV.A for the moving window and the averaging procedure apply in a similar fashion to the CTF-based approach.

C. Hilbert-Transform-Based Approach

The third approach proposed in this paper is based on the Hilbert transform. A possible way to describe the Hilbert transform [18] $\tilde{y}(t)$ of a real-valued signal $y(t)$ is through the definition of the analytical signal $z(t)$:

$$z(t) = y(t) + j\tilde{y}(t)$$

or, in polar coordinates,

$$z(t) = A(t)je^{j\theta(t)}$$

where $A(t)$ is the envelope signal and $\theta(t)$ is the instantaneous phase of $y(t)$. A third quantity denominated instantaneous frequency can also be defined as

$$f(t) = \frac{1}{2\pi}\frac{\mathrm{d}\theta(t)}{\mathrm{d}t}$$

Standing by these definitions, it follows that one possible way to describe the Hilbert transform of a real-valued signal is

$$\tilde{y}(t) = H[x(t)] = \mathrm{Im}[z(t)]$$

that is, calculating the imaginary part of the analytic signal $z(t)$.

One of the most interesting features of the HT consists in the fact that it retains the time information that, otherwise, in other approaches like the DFT or the CTF, is completely discarded. This constitutes a major benefit in the proposed procedure and will be addressed in further details later on in this paper.

It can be seen from the block diagram in Fig. 7 that the outputs collected at the two sensors are first processed through a series of zero phase-shift bandpass filters centered at the superharmonic frequencies to separate the component of the time response due to a specific harmonic. Then, each signal is separately processed through the Hilbert transform to get the instantaneous phase $\varphi_{1,n}(t)$ and $\varphi_{2,n}(t)$ associated with each harmonic. Successively, the phase difference $\Delta\varphi_n$ is calculated and fed into the damage detection algorithm block that will produce an estimate of the crack location based on each superharmonic component. Finally, the array of the estimated location is linearly averaged to get the final estimate of the crack location.

V. Numerical Results

Analytical simulations have been carried out to estimate the capabilities and the performances of the proposed algorithm along with the data postprocessing approaches. The time response of the damaged structure has been generated through the FE model discussed in Sec. III.E and the crack location has been estimated

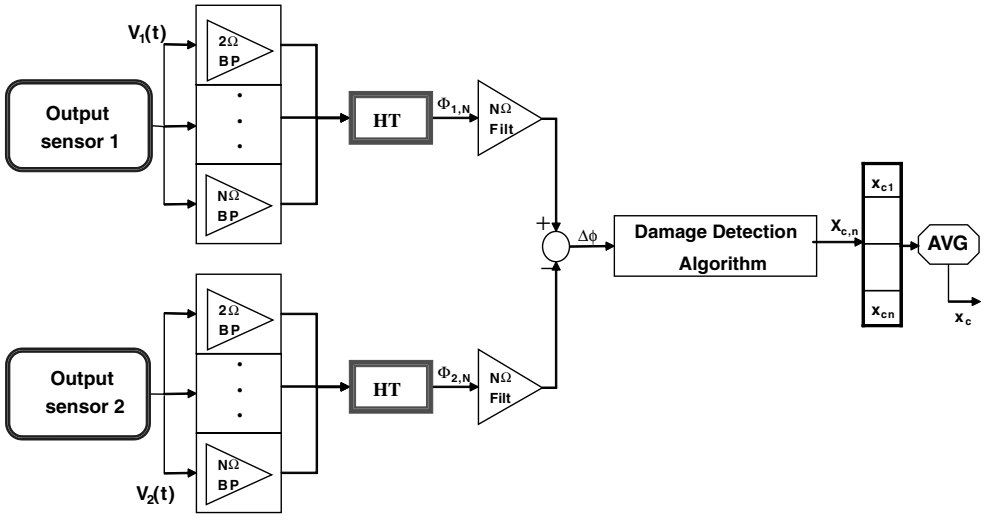

Fig. 7 Block diagram of the Hilbert-transform-based approach.

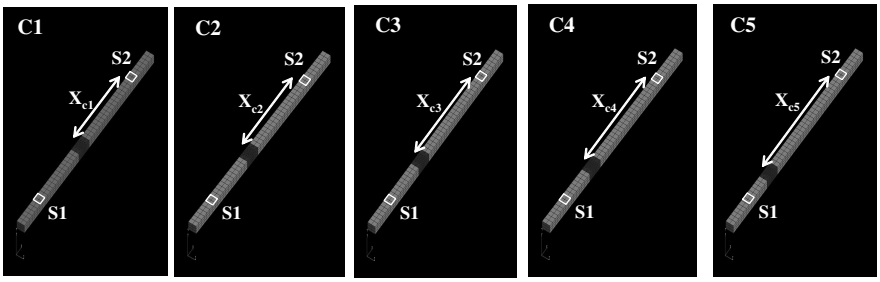

Fig. 8 Schematic of the five crack configurations.

using the three different postprocessing procedures discussed in Sec. IV.

In particular, five different crack configurations have been considered and compared. Each configuration corresponds to a specific FE model, including one breathing crack with a different location along the longitudinal axis but with the same geometrical properties (2×0.86 mm), as shown in Fig. 8. It can be noted that, starting from configuration C1 up to configuration C5, the crack is shifted progressively farther from sensor S2.

The external excitation used to interrogate the structure is a sinusoidal axial load with a frequency equal to 40 kHz and a zero to peak amplitude equal to 100 N.

A. Discrete-Fourier-Transform-Based Data Postprocessing

The time response produced by the FE model for the five different configurations are postprocessed through the procedure proposed in Sec. IV.A. Table 2 shows a comparison between the real and the estimated locations of the crack.

It can be noted that, although the configurations C1 and C2 are fairly well predicted, the accuracy of the estimation starts deteriorating from C3 to C5. Moreover, for the C5 configuration, we observed a wrong estimate of the sign of the $\Delta\varphi$, which results in an erroneous prediction of the portion of the beam where the crack is located. This inconsistent behavior in the prediction capabilities of the algorithm is even more accentuated when changing the windowing parameters used for the moving window approach.

Different causes have been identified to explain this phenomenon. The DFT approach calculates the relative phase treating the signal coming from the two sensors as decorrelated signals. This may result in an amplification of eventual systematic errors leading, therefore, to an erroneous estimate of the relative phase difference. This aspect becomes even more important considering that the estimated location is considerably affected by the choice of the windowing parameters and from the frequency resolution of the spectrum. The windowing parameters, in fact, cannot be matched for both the signals to minimize the leakage effect. This produces considerable fluctuations in the predicted values depending on the initial choice of the window.

Moreover, the DFT approach is extremely sensitive to the choice of the frequency resolution. Because of computational limitations related to the solution of the FE model in a nonlinear time domain, we could not achieve a frequency resolution lower than 20 Hz. However, it can be easily shown through a set of analytically generated sine waves (reproducing a condition similar to the one produced by the model structural response) with a known phase difference that, in this specific case, the DFT achieves a good accuracy for the phase estimate only when using a frequency resolution of 1 Hz or lower. The authors believe that the frequency resolution issue can be easily overcome when acquiring experimental data where the frequency step can be dropped down to 1 Hz or even lower. However, for numerically generated data, this is still a major problem preventing the use of this algorithm for prediction purposes.

Finally, the ratio S_D/S_{SH} between the amplitude of the driving frequency S_D versus the amplitude of the superharmonic component S_{SH} has also been found to play a major role in the accuracy of the DFT-based algorithm. In particular, it has been found that the higher this ratio, the lower the maximum achievable accuracy.

B. Cross-Transfer-Function-Based Data Postprocessing

To overcome the issues encountered with the DFT-based methodology, we moved to a CTF-based approach, described in Sec. IV.B, to postprocess the structural response. A summary of the estimated crack locations produced by this approach is shown in Table 3.

It can be noted that a good agreement between the actual and the estimated location is obtained for configurations C2, C4, and C5, with a maximum percentage error of 5.1% corresponding to configuration C5. Although, configurations C1 and C3 show a higher error (greater than 20%) with respect to the other configurations, a major improvement is obtained through the CTF approach when compared with the DFT. For the whole set of configurations, in fact, the term $\mathrm{sgn}(\Delta\varphi)$ is always well predicted resulting, therefore, in the correct estimate of the crack in the right portion of the beam. The improved consistency of the results is due to the fact that the relative phase $\Delta\varphi$ is now calculated extracting the phase associated with the cross transfer function between the two signals. This approach is much more robust to systematic error and provides a higher accuracy (compared with the DFT) even in presence of a high S_D/S_{SH} ratio.

However, some of the problems discovered in the DFT approach still persist. In particular, it has been found that the accuracy is still sensitive to the choice of the windowing parameters, giving rise to an oscillation in the values of the predicted location dependent on their initial choice. Also, in this approach, the frequency resolution is limiting the overall accuracy.

C. Hilbert-Transform-Based Data Postprocessing

As described in Sec. IV.C, the third data postprocessing approach proposed in this paper is based on the Hilbert transform. Table 4 shows the locations of the crack for the five different configurations obtained through this approach.

Table 2 Comparison between real and estimated locations calculated through the DFT approach

	Real location, mm	Estimated location, mm	Error, %
C1	60	59.53	0.8
C2	68	70.63	3.8
C3	76	53.89	−29.1
C4	84	55.14	−34.4
C5	92	46.58	50.6

Table 3 Comparison between real and estimated locations calculated through the CTF approach

	Real location, mm	Estimated location, mm	Error, %
C1	60	74.43	24.0
C2	68	70.93	4.3
C3	76	60.04	−21.0
C4	84	83.33	−0.8
C5	92	96.68	5.1

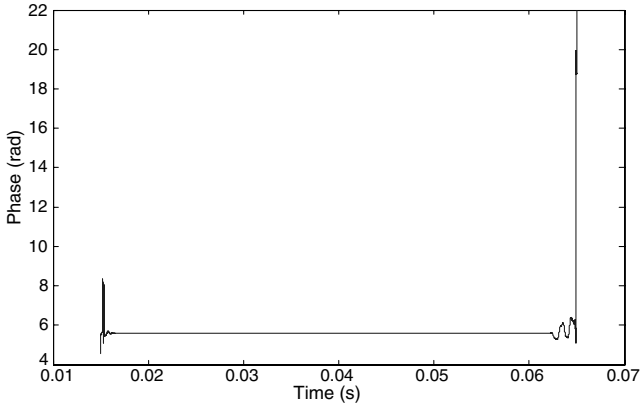

Fig. 9 Phase difference calculated through the Hilbert transform for the 2Ω harmonic.

With the exception of C2, where the error on the estimated location is around 20%, the algorithm shows a fairly good prediction of the crack location for the other configurations. Nevertheless, the most interesting outcome of these results is not the overall accuracy but the observed consistency of the results versus the choice of the windowing parameters. In fact, the major advantage produced by this approach (if compared with the CTF or the DFT) is that the accuracy of the results is not sensitive to the windowing parameters. Regardless of the choice for the initial window, in fact, the results are always very consistent and the term $\mathrm{sgn}(\Delta\varphi)$ is always correctly estimated. Moreover, the HT approach has proven to be computationally much faster than the previous approaches, being, therefore, a more suitable algorithm for real-time damage detection.

The improved consistency of the results produced by this algorithm is explained by the fact that the Hilbert transform provides, as described in Sec. IV.C, the history of the instantaneous phase versus time for each specific superharmonic. This results in two major advantages. First, we can keep track of the phase oscillation due to the effects either of the reflected waves or of the nonlinear behavior of the system. Second, the average value of the phase can be better estimated due to the extended set of phase values associated with each specific frequency, as opposed to the single value produced by the CTF or DFT approaches. This concept is better clarified by Fig. 9 which shows the relative phase difference for the 2Ω harmonic calculated through the HT approach. Whereas the CTF approach provides only one value for the estimated phase difference at the specified frequency, the Hilbert transform gives $N = (t_f - t_0)/\Delta T$ samples. In this way, even a simple linear average is able to reduce the effect of the reflected waves and phase oscillations due to the nonlinearities, allowing a good estimate of the $\Delta\varphi$. The results shown in Table 4 have been calculated using the first three superharmonic components (i.e., 2Ω, 4Ω, and 6Ω) for which the ratio $S_D/S_{\mathrm{SH}} \leq 10^4$. Harmonics greater than 6Ω were too weak to be retained.

Finally, it is expected that the accuracy of this approach can be improved, extending the set of data by performing multiple interrogation at different driving frequencies and exploiting the information associated with a larger set of superharmonics.

Table 4 Comparison between real and estimated locations calculated through the HT approach

	Real location, mm	Estimated location, mm	Error, %
C1	60	66.92	11.5
C2	68	81.57	19.9
C3	76	77.79	2.3
C4	84	73.17	−12.9
C5	92	86.37	−6.2

VI. Conclusions

A damage detection technique able to identify the location of a breathing crack in an isotropic rod is presented. The procedure takes advantage of the nonlinear behavior proper of a breathing-crack-type defect, allowing the localization of the damage relying only on real-time measurements of the structural response.

To test the performances of the localization algorithm, a specific nonlinear finite element model integrating a breathing crack has been developed. The model has been solved for the nonlinear time response to generate the set of data needed as input for the detection algorithm. Three different data postprocessing approaches integrating the proposed localization technique have been developed and compared. These approaches rely, respectively, on the use of the discrete Fourier transform, the cross transfer function, and the Hilbert transform to estimate the relative phase difference between the collected signals at the superharmonic frequencies.

The three approaches have been compared based on their capability to correctly characterize five different crack configurations, both in terms of the absolute percentage error and the right estimate of the term $\mathrm{sgn}(\Delta\varphi)$, which characterizes the portion of the rod where the crack is located. The Hilbert-transform-based approach has proven to be the most successful technique due to its ability to provide information about the instantaneous phase of the signal. In particular, its capability to provide an extended set of data for each harmonic, along with its considerable robustness against the choice of the postprocessing parameters and its reduced computational time, makes it a suitable candidate for data analysis in the present damage detection approach.

Overall, the results illustrated in this paper showed that the proposed methodology has the potential to successfully identify the location of a breathing-crack-type defect without relying either on a database or on an accurate FE model of the structure. Although the results obtained for some crack configurations show a percentage error close to 20%, it is expected that the use of an extended set of data produced through a multiple frequency interrogation could considerably improve the overall accuracy. Also, the results presented in this paper highlighted the existence of some key parameters, having a considerable impact on the performances of the damage detection algorithm. In particular, the relation between the driving frequency, the amplitude of the response at the superharmonic frequencies, and the crack location should be further investigated to provide a rigorous procedure for the selection of the interrogation frequency. In the future, a more rigorous selection criterion should be established to identify the proper subset of superharmonics to be retained in the postprocessing approach.

As a concluding remark, it should be noted that, although the current technique has been applied to a specific type of defect (i.e., a breathing crack), it is expected that this procedure could be applied in a similar fashion to other kind of faults exhibiting similar nonlinear behavior. As an example, in fact, the phenomenon of the superharmonic generation in a structure subjected to an external dynamic excitation has also been observed for closing delamination in composite material [19].

Acknowledgments

The authors wish to acknowledge the Centre for Rotorcraft Innovation which provided the grant to support this research. The first author wishes to thank Martin Trethewey for his valuable contribution to the data postprocessing.

References

[1] Doebling, S. W., Farrar, C. R., and Prime, M. B., "A Summary Review of Vibration-Based Damage Identification Methods," *Shock and Vibration Digest*, Vol. 30, No. 2, March 1998, pp. 91–105. doi:10.1177/058310249803000201

[2] Doebling, S. W., Farrar, C. R., Prime, M. B., and Shevitz, D. W., "Damage Identification and Health Monitoring of Structural and Mechanical Systems from Changes in Their Vibration Characteristics: A Literature Review," Los Alamos National Lab., Rept. LA-13070-MS, 1996.

[3] Montalvao, D., Maia, N. M. M., and Ribeiro, A. M. R., "A Review of Vibration-Based Structural Health Monitoring with Special Emphasis on Composite Materials," *Shock and Vibration Digest*, Vol. 38, No. 4, July 2006, pp. 295–324. doi:10.1177/0583102406065898

[4] Salawu, O. S., "Detection of Structural Damage Through Changes in Frequency: A Review," *Engineering Structures*, Vol. 19, No. 9, 1997, pp. 718–723. doi:10.1016/S0141-0296(96)00149-6

[5] Sohn, H., "Effects of Environmental and Operational Variability on Structural Health Monitoring," A Special Issue of *Philosophical Transactions of the Royal Society of London, Series A: Mathematical and Physical Sciences* on Structural Health Monitoring, Vol. 365, No. 1851, Feb. 2007, pp. 539–560. doi:10.1098/rsta.2006.1935

[6] Shen, M. H., and Chu, Y. C., "Vibrations of Beams with a Fatigue Crack," *Computers and Structures*, Vol. 45, No. 1, 1992, pp. 79–93. doi:10.1016/0045-7949(92)90347-3

[7] Solodov, I., Wackerl, J., Pfleiderer, K., and Busse, G., "Nonlinear Self-Modulation and Subharmonic Acoustic Spectroscopy for damage Detection and Location," *Applied Physics Letters*, Vol. 84, No. 26, 2004, pp. 5386–5388. doi:10.1063/1.1767283

[8] Nayfeh, A. H., and Mook, D. T., *Nonlinear Oscillations*, Wiley-Interscience, New York, 1993.

[9] Doyle, J. F., *Wave Propagation in Structures*, Springer–Verlag, New York, 1989.

[10] Doyle, J. F., "An Experimental Method for Determining the Location and Time of Initiation of an Unknown Dispersing Pulse," *Experimental Mechanics*, Vol. 27, No. 3, 1987, pp. 229–233. doi:10.1007/BF02318087

[11] Bayly, P. V., "On the Spectral Signature of Weakly Bilinear Oscillators," *Journal of Vibration and Acoustics*, Vol. 118, No. 3, 1996, pp. 352–361. doi:10.1115/1.2888190

[12] Sundermeyer, J. N., and Weaver, R. L., "On Crack Identification and Characterization in a Beam by Nonlinear Vibration Analysis," *Journal of Sound and Vibration*, Vol. 183, No. 5, 1995, pp. 857–871. doi:10.1006/jsvi.1995.0290

[13] Musil, M., "Localization and Quantification of Breathing Crack," *Transactions of the American Society of Mechanical Engineers*, Vol. 128, 2006, pp. 458–462.

[14] Sinha, J. K., and Friswell, M. I., "Simulation of the Dynamic Response of a Cracked Beam," *Computers and Structures*, Vol. 80, Nos. 18–19, 2002, pp. 1473–1476. doi:10.1016/S0045-7949(02)00098-6

[15] Luzzato, E., "Approximate Computation of Non-Linear Effects in a Vibrating Cracked Beam," *Journal of Sound and Vibration*, Vol. 265, No. 4, 2003, pp. 745–763. doi:10.1016/S0022-460X(02)01562-6

[16] Douka, E., and Hadjileontiadis, L. J., "Time-Frequency Analysis of the Free Vibration Response of a Beam with a Breathing Crack," *NDT&E International: Independent Nondestructive Testing and Evaluation*, Vol. 38, No. 1, 2005, pp. 3–10. doi:10.1016/j.ndteint.2004.05.004

[17] Mickens, R. E., *An Introduction to Nonlinear Oscillations*, Cambridge Univ. Press, Cambridge, England, U.K., 1981.

[18] Bendat, J. S., and Piersol, A. G., *Random Data: Analysis and Measurements Procedures*, Wiley, New York, 2000.

[19] Zak, A., Krawczuk, M., and Ostachowicz, W., "Vibration of a Laminated Composite Plate with Closing Delamination," *Journal of Intelligent Material Systems and Structures*, Vol. 12, No. 8, 2001, p. 545. doi:10.1177/10453890122145320

A. Roy
Associate Editor